Nodal band-off-diagonal superconductivity in twisted graphene superlattices

Maine Christos, ¹ Subir Sachdev, ¹ and Mathias S. Scheurer ²

¹Department of Physics, Harvard University, Cambridge MA 02138, USA

²Institute for Theoretical Physics, University of Innsbruck, Innsbruck A-6020, Austria

The superconducting state and mechanism are among the least understood phenomena in twisted graphene systems. For instance, recent tunneling experiments indicate a transition between nodal and gapped pairing with electron filling, which is not naturally understood within current theory. We demonstrate that the coexistence of superconductivity and flavor polarization leads to pairing channels that are guaranteed by symmetry to be entirely band-off-diagonal, with a variety of unusual consequences: most notably, the pairing invariant under all symmetries can have protected nodal lines or be fully gapped, depending on parameters, and the band-off-diagonal chiral d-wave state exhibits transitions between gapped and nodal regions upon varying the chemical potential. We demonstrate that nodal band-off-diagonal pairing can be the leading state when only phonons are considered, and is also uniquely favored by fluctuations of a time-reversal-symmetric intervalley-coherent order motivated by recent experiments. Consequently, band-off-diagonal superconductivity allows for the reconciliation of several key experimental observations in graphene moiré systems.

I. INTRODUCTION

The fascinating physics [1, 2] of correlated graphene moiré superlattices, such as twisted bilayer (TBG) and twisted trilayer graphene (TTG), has generated extensive efforts to uncover the mysteries of their phase diagrams. Much progress has been made towards understanding their normal-state physics, including the correlated insulating phases [3–18], and the reset behavior [19, 20], which is believed to be associated with the onset of flavor polarization, appears in the same density range of and can coexist with superconductivity [13, 19–34]. However, the form and symmetry of the superconducting order parameter and the pairing glue are still unknown, despite significant theoretical efforts [27–30, 33, 35–47].

Tunneling conductance measurements taken within the superconducting state reveal V-shaped density of states (DOS) [48, 49] which can become U-shaped at other electron concentrations [49]. Setting aside the possibility of thermal fluctuations as origin [50], this implies a transition from nodal to fully gapped superconductivity. For a consistent microscopic theoretical understanding, this provides the following challenges: (i) electron-phonon coupling—a widely discussed [33, 35-40] pairing mechanism in TBG and TTG—will typically mediate an entirely attractive interaction in the Cooper channel, with leading pairing state that transforms trivially under all symmetries and is thus fully gapped [51, 52]. (ii) Even when the low-energy interactions favor an irreducible presentation (IR), e.g., E of C_3 , with nodal basis functions (p- or d-wave), the generically fully gapped chiral configuration wins over the nodal nematic one within mean-field. (iii) Even if we assume that the nodal state is energetically favored, e.g., due to significant corrections beyond mean-field [27, 53–55], one is still left to explain why there is a transition to another, fully gapped superconductor upon changing the filling.

In this work, we show that the combination of flavor polarization and the representations of the symmetries in the flat bands of TBG and TTG allow for pairing channels that are *completely* off-diagonal in the flat bands and that such band-off-diagonal states can naturally reconcile all three key challenges (i-iii). More specifically, we find two distinct band-off-diagonal states: one of them transforms under the trivial representation A of the system's point group C_6 (or one of $A_{1,2}$ of D_6 if we set the displacement field to zero) but will nonetheless have a symmetryprotected nodal lines, akin to Bogoliubov Fermi surfaces discussed in [56, 57]. The second off-diagonal state transforms under a two-dimensional IR (E_2 of C_6). Its associated chiral state, $E_2(1,i)$, which is favored in mean-field over the nematic one, has the unique property of exhibiting nodal lines or being fully gapped depending on the filling fraction, even when the order parameter is kept fixed. We supplement our general symmetry arguments and phenomenological models with Hartree-Fock (HF) calculations on the continuum model, studying a variety of different pairing mechanisms. We find that nodal band-off-diagonal pairing is favored by the optical A_1 and B_1 phonon modes and by fluctuations of a time-reversal symmetric intervalley coherent (T-IVC) state (the T-IVC state has Kekulé order on the graphene scale [58–60]). Evidence for the former has been provided by recent photoemission experiments [61] while evidence for the latter has been provided by recent STM experiments [7]. Furthermore, also fluctuations of a time-reversal-symmetric sublattice polarized state (SLP+) are attractive in the band-off-diagonal channel. We also show when fluctuations of both the strong coupling T-IVC ground state and of a nematic, time-reversal symmetric IVC order [62] are present, the leading instability is either our A_2 state or an E_1 state which may also be nodal, with the winner being determined by the relative amount of nematic IVC and T-IVC fluctuations.

II. RESULTS

A. Possible pairing states

Let us begin by classifying the superconducting instabilities in graphene moiré systems in the limit where the low-energy bands are spin polarized but allowing for multiple bands. We denote the spinless low-energy fermionic creation operators by $c_{\mathbf{k},\alpha,\eta}$ with momentum \mathbf{k} in valley $\eta=\pm$, and of band index α labeling the upper $(\alpha=+)$ and lower $(\alpha=-)$ quasi-flat bands. As a result of two-fold rotational symmetry, C_{2z} , along the out-of-plane (z) direction or effective spinless time-reversal symmetry, Θ , the non-interacting band structure $\xi_{\mathbf{k},\alpha,\eta}$ obeys $\xi_{\mathbf{k},\alpha,\eta}=\xi_{-\mathbf{k},\alpha,-\eta}\equiv \xi_{\eta\cdot\mathbf{k},\alpha}$ and intervalley pairing is expected to dominate. A general pairing order parameter in the inter-valley channel couples as

$$\mathcal{H}_{p} = \sum_{\boldsymbol{k}, \eta = \pm, \alpha, \alpha'} c_{\boldsymbol{k}, \alpha, \eta}^{\dagger} \left(\Delta_{\boldsymbol{k}, \eta} \right)_{\alpha, \alpha'} c_{-\boldsymbol{k}, \alpha', -\eta}^{\dagger} + \text{H.c.}, \quad (1)$$

where the order parameter $\Delta_{\mathbf{k},\eta} = -\Delta_{-\mathbf{k},-\eta}^T$ is a matrix in band space. The physical spin texture of the superconductor is entirely determined by the form of the underlying normal state's polarization: if the spins are aligned in the two valleys, the superconductor is a non-unitary triplet, while anti-alignment [24, 28] leads to a singlet-triplet admixed state [13, 27, 28]. We here focus on aligned spins for simplicity.

We will classify the pairing states according to the irreducible representations (IRs) of the system's point group D_6 , which is generated by six-fold rotations (C_{6z}) along the z axis and two-fold rotation symmetry (C_{2x}) along the in-plane x axis. Note a displacement field $(D_0 \neq 0)$ breaks the in-plane rotations leading to the point group C_6 . Importantly, all IRs of D_6 and C_6 are either even or odd under C_{2z} . Choosing the phases of the Bloch states such that C_{2z} acts as $c_{\mathbf{k},\alpha,\eta} \to c_{-\mathbf{k},\alpha,-\eta}$, it holds

$$C_{2z}: \Delta_{\mathbf{k},\eta} \longrightarrow \Delta_{-\mathbf{k},-\eta} = -\Delta_{\mathbf{k},\eta}^T.$$
 (2)

This immediately implies that the pairing states in all IRs even under C_{2z} $(A_1, A_2, E_2 \text{ of } D_6)$ must be antisymmetric in band space and, thus, entirely band offdiagonal, whereas the order parameters of the other IRs (B_1, B_2, E_1) are symmetric and can contain both band-diagonal and band-off-diagonal components. While superconducting order parameters with finite band-offdiagonal components are rather common in multi-band systems, the existence of pairing states that are constrained to be *entirely* band-off-diagonal is rather unique and follows from the combination of C_{2z} symmetry and the spin polarization in the normal state. Note that this observation is consistent with the classification in Ref. 27 where all C_{2z} -even intraband pairings were found to have no triplet component. In conventional dispersive multiband systems, one would expect these purely inter-band

TABLE I: Summary of pairing states in spin-polarized flat bands. Here $\chi_{\mathbf{k}}$ ($\hat{\chi}_{\mathbf{k}}$) is a real-valued (real and symmetric) MBZ-periodic function invariant under C_{3z} . Furthermore, $X_{\mathbf{k}}$ and $Y_{\mathbf{k}}$ ($\hat{X}_{\mathbf{k}}$ and $\hat{Y}_{\mathbf{k}}$) transform as x and y under D_3 , generated by C_{3z} and C_{2x} , while also being real (and symmetric). The third column indicates the type of nodes on a generic Fermi surface for sufficiently small/large order-parameter magnitudes and the last column shows which states merge when $D_0 \neq 0$, reducing the point group from D_6 to C_6 .

IR of D_6	$\Delta_{m{k},\eta} = \Delta_{-m{k},-\eta}^T$	nodes	IR of C_6
A_1	$\sigma_y \chi_{\eta \cdot \mathbf{k}}, \chi_{C_{2x}\mathbf{k}} = -\chi_{\mathbf{k}}$	line/point	A
A_2	$\sigma_y \chi_{\eta \cdot \mathbf{k}}, \chi_{C_{2x}\mathbf{k}} = \chi_{\mathbf{k}}$	line/none	A
$E_2(1,0)$	$\sigma_y X_{\eta \cdot oldsymbol{k}}$	line/point	$E_2(1,0)$
$E_2(0,1)$	$\sigma_y Y_{\eta \cdot oldsymbol{k}}$	line/point	$E_2(1,0)$
$E_2(1,i)$	$\sigma_y \left(X_{\eta \cdot \mathbf{k}} + i Y_{\eta \cdot \mathbf{k}} \right)$	line/none	$E_2(1, i)$
B_1	$\eta \hat{\chi}_{\eta \cdot \mathbf{k}}, \sigma_z \hat{\chi}_{C_{2x}\mathbf{k}} \sigma_z = \hat{\chi}_{\mathbf{k}}$	none	B
B_2	$\eta \hat{\chi}_{\eta \cdot \mathbf{k}}, \sigma_z \hat{\chi}_{C_{2x}\mathbf{k}} \sigma_z = -\hat{\chi}_{\mathbf{k}}$	point	B
$E_1(1,0)$	$\eta \hat{X}_{m{\eta}\cdotm{k}}$	point	$E_1(1,0)$
$E_1(0,1)$	$\eta \hat{Y}_{m{\eta}\cdotm{k}}$	point	$E_1(1,0)$
$E_1(1,i)$	$\eta \left(\hat{X}_{\eta \cdot \mathbf{k}} + i \hat{Y}_{\eta \cdot \mathbf{k}} \right)$	none	$E_1(1,i)$

states to be suppressed; however, graphene moiré systems have almost flat bands where the bandwidth can be comparable or smaller than the interactions scale and the associated energy penalty can be overcompensated, as we will demonstrate explicitly below.

Choosing the phase conventions of the Bloch states such that C_{2x} and C_{3z} act as $c_{\mathbf{k},\alpha,\eta} \to \sigma_z c_{(k_x,-k_y),\alpha,\eta}$ and $c_{\mathbf{k},\alpha,\eta} \to c_{C_{3z}\mathbf{k},\alpha,\eta}$, respectively, the resulting candidate order parameters are summarized in Table I. Note that a momentum-independent representation of C_{2x} must be σ_z due to the band's eigenvalues at the Γ -M line, which in turn is connected to the topological obstruction of the flat bands [63]. The reality (Hermiticity) constraint in Table I on χ , X, and Y ($\hat{\chi}$, \hat{X} , and \hat{Y}) comes from the residual spinless time-reversal symmetry Θ of the normal state [64, 65]. The two two-dimensional IRs $E_{1,2}$ are each associated with three pairing states—two nematic phases $E_{1,2}(1,0)$, $E_{1,2}(0,1)$ and one chiral state $E_{1,2}(1,i)$.

B. Spectral properties

We here have the rather unique situation that there are pairing channels, associated with the IRs $A_{1,2}$ and E_2 , where the pairing is constrained by C_{2z} to be entirely band off-diagonal. One immediate very unusual consequence is that the superconducting order parameter transforming under the trivial representation (A_1) has a symmetry-imposed line of zeros along the Γ -M line. This is related to the topology-induced non-

trivial representation of C_{2x} in band space. We refer to Ref. 39 for the discussion of other topological nodal points for pairing in obstructed TBG bands. As we will show next, band-off-diagonal pairing leads to additional unusual spectral properties with far reaching consequences for graphene moiré systems. To this end, consider the following effective Hamiltonian, $\mathcal{H}_{\sigma_y} =$ $\sum_{\boldsymbol{k}} c^{\dagger}_{\boldsymbol{k},\alpha,\eta} c_{\boldsymbol{k},\alpha,\eta} \xi_{\eta\cdot\boldsymbol{k},\alpha} + \sum_{\boldsymbol{k}} [\Delta_{\boldsymbol{k}} \, c^{\dagger}_{\boldsymbol{k},+} \sigma_y c^{\dagger}_{-\boldsymbol{k},-} + \text{H.c.}],$ where the scalar function $\Delta_{\boldsymbol{k}}$ describes the form of pairing. We will here study two cases which are conventionally considered to be fully gapped, (i) a momentum-independent "swave state" (A_2 pairing in Table I) where $\Delta_{\mathbf{k}} = \Delta_0$ and (ii) a "chiral d-wave" state, or more precisely an $E_2(1,i)$ state, where $\Delta_{\mathbf{k}} = \Delta_0(X_{\mathbf{k}} + iY_{\mathbf{k}})$ with $(X_{\mathbf{k}}, Y_{\mathbf{k}})$ being smooth, MBZ-periodic functions transforming as (x, y)under C_{3z} . Furthermore, we parameterize the dispersion, $\xi_{\eta \cdot \mathbf{k}, \alpha}$, of the two flat bands $(\alpha = \pm)$ in valley $\eta = \pm$ as $\xi_{\mathbf{k},\alpha} = \epsilon_{\mathbf{k}} - \mu + \alpha \, \delta_{\mathbf{k}}$, where $\epsilon_{\mathbf{k}}$ and $\delta_{\mathbf{k}}$ are C_{3z} (and, for $D_0 = 0, C_{2x}$) symmetric functions.

The Bogoliubov spectrum of \mathcal{H}_{σ_y} has four bands, given by $\pm \delta_{\mathbf{k}} \pm \sqrt{(\epsilon_{\mathbf{k}} - \mu)^2 + |\Delta_{\mathbf{k}}|^2}$. Consequently, the excitation gap at momentum \mathbf{k} reads as

$$\Delta E_{\mathbf{k}} = \left| |\delta_{\mathbf{k}}| - \sqrt{(\epsilon_{\mathbf{k}} - \mu)^2 + |\Delta_{\mathbf{k}}|^2} \right|, \tag{3}$$

which is shown in Fig. 1(a), and therefore exhibits nodes where $|\delta_{\mathbf{k}}| = \sqrt{(\epsilon_{\mathbf{k}} - \mu)^2 + |\Delta_{\mathbf{k}}|^2}$. As long as the band structure has Dirac points, there are points k_D in the Brillouin zone with $\delta_{\mathbf{k}_D} = 0$, associated with the blue cross in Fig. 1(a). Furthermore, for a metallic normal state, μ must be within the bandwidth and, hence, there must be a region R in momentum space where $|\delta_{\mathbf{k}}| > |\epsilon_{\mathbf{k}} - \mu|$. For the momentum-independent A_2 state, $\Delta_{\mathbf{k}} = \Delta_0$, this implies that there exists $\Delta_0^c > 0$ such that there is $k^* \in R$ with parameters (such as the blue circle) above the red solid line in Fig. 1(a) as long as $|\Delta_0| < \Delta_0^c$. By continuity, this means that there must be a nodal point on any line connecting k_D and k^* . Consequently, for μ within the bandwidth and $\delta_{k_D} = 0$ for some k_D , the A_2 will always have a nodal line if $|\Delta_0|$ is sufficiently small. We illustrate this in Fig. 1(b) using a toy model with $\delta_{\mathbf{k}} = t \left| 1 + e^{i\mathbf{a}_1 \cdot \mathbf{k}} + e^{-i\mathbf{a}_2 \cdot \hat{\mathbf{k}}} \right|$ and $\epsilon_{\boldsymbol{k}} = t' \sum_{j=1}^{3} \cos \boldsymbol{a}_j \cdot \boldsymbol{k}, \ \boldsymbol{a}_j = [C_{3z}]^{j-1} (\sqrt{3}, 0)^T;$ like in single-layer graphene and twisted graphene systems, the Dirac cones in this model occur at the K and K' points [see red dots in the upper right panel in Fig. 1(b)]. This leads to the first unexpected conclusion that, for any pairing mechanism, including conventional electron-phonon coupling, the leading instability either has nodal lines in a finite region below T_c or transforms non-trivially under the symmetries of the normal state. For electron-phonon pairing (or pairing mediated by the fluctuations of any time-reversal-symmetric order parameter [52], such as the T-IVC state) this is particularly unexpected since it is generally believed to always lead to a fully gapped state

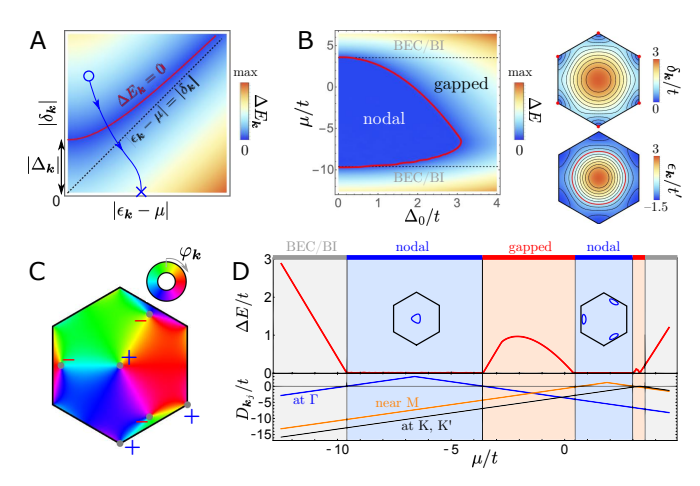


FIG. 1: Spectral properties of interband pairing. (a) k-local gap of interband superconductivity according to Eq. (3), where the red line indicates nodal points. If the band structure has Dirac points, there will be a point on the horizontal axis (blue cross). Consequently, if there is another momentum point located above the red line (blue circle), continuity of the Hamiltonian implies a nodal point on any path connecting the two momenta. (b) Gap of the isotropic A_2 state and $\delta_{\mathbf{k}}$, $\epsilon_{\mathbf{k}}$ (zeros indicated in red) for the normal-state toy model defined in the text. (c) Complex phase $\varphi_{\mathbf{k}} = \arg(X_{\mathbf{k}} + iY_{\mathbf{k}})$ for leading basis function with small subleading corrections. (d) Shows the gap of the chiral d-wave $E_2(1,i)$ state with $\Delta_0 = 1.5t$ and the value of $D_{\boldsymbol{k}_j} := |\delta_{\boldsymbol{k}_j}| - |\epsilon_{\boldsymbol{k}_j} - \mu| \text{ for } \boldsymbol{k}_j \text{ at the three}$ symmetry-in-equivalent vortices in (c) as a function of μ . We took t' = -2.2t, t > 0, in (b,d).

that transforms trivially under all symmetries. In fact, this can be proven in general terms [51, 52], even for spinorbit-split Fermi surfaces and beyond mean-field theory [52]. The crucial difference to these works, however, is that *spinful* time-reversal is broken in our case such that the Fermi-Dirac constraint is inconsistent with a nonsign-changing, band-diagonal pairing state. This leads to the unique situation that although electron-phonon coupling will lead to entirely attractive interactions in the Cooper channel, the superconducting energetics is frustrated: the dominant pairing state is determined by whether the energetic loss due to non-resonant band-offdiagonal Cooper pairs (A_2 pairing) or the costs from sign changes of the order parameter (such as B_1) are less harmful. We will demonstrate this explicitly by a model calculation in Sec. II E below, where either A_2 or B_1 is dominant, depending on the form of the electron phonon coupling.

Let us first, however, discuss the general spectral properties of the "chiral d-wave" state which is canonically expected to be fully gapped as long as the Fermi surfaces do not cross the zeros of $X_{\boldsymbol{k}}+iY_{\boldsymbol{k}}$. Three of these zeros have to be at the Γ, K , and K' points as a consequence of C_{3z} symmetry. In the absence of fine-tuning, $X_{\boldsymbol{k}}+iY_{\boldsymbol{k}}$

will have vortices at these points with the lowest possible vorticity v = +1 (note that v = -1 is inconsistent with C_{3z}). As can be seen in Fig. 1(c), where we show the phase of $X_{\mathbf{k}} + iY_{\mathbf{k}}$ using an admixture of the two lowest-order terms, the net vorticity of +3 at these highsymmetry points has to be compensated by anti-vortices at generic momenta. The lowest possible number is three C_{3z} -related vortices, which appear near the M points in Fig. 1(c). If it holds $|\delta_{\mathbf{k}}| > |\epsilon_{\mathbf{k}} - \mu|$ at any of these zeros $k = k_i$, we obtain a point above the red line in Fig. 1(a) and, thus, a nodal point along any contour between that k_j and k_D ; as opposed to the A_2 state, this holds irrespective of the value of Δ_0 and therefore all the way to zero temperature. In summary, we find that also the $E_2(1,i)$ "chiral d-wave" state is not generically fully gapped but instead will exhibit a nodal line encircling any zero k_j of $X_k + iY_k$ with $|\delta_{k_j}| > |\epsilon_{k_j} - \mu|$. This leads to an interesting filling dependence of the superconducting gap, as we illustrate in our toy model in Fig. 1(d) along with the criterion $D_{\mathbf{k}_j} := |\delta_{\mathbf{k}_j}| - |\epsilon_{\mathbf{k}_j} - \mu| > 0$ evaluated at the vortices at Γ , K/K', and near M. Depending on μ , $D_{\mathbf{k}}$ is positive only near the Γ point or only in a region surrounding the vortices close to the M points, leading to nodal lines encircling Γ and near the M points, respectively, as shown in the inset of Fig. 1(d). These regimes are separated by a fully gapped region where $D_{\mathbf{k}} < 0$ for all \mathbf{k} , which could naturally explain the fully gapped to nodal transition seen in tunneling experiments [49] when the filling fraction is changed. Note that $D_{\mathbf{k}_i} = -|\epsilon_{\mathbf{k}_i} - \mu| \leq 0$ for \mathbf{k}_i at the K and K' points. In Fig. 1(d), $D_K = D_{K'}$ vanishes close to the top of the band, which simply means that the Fermi surfaces cross the K, K' points and the superconductor has nodal points for this fine-tuned value of the chemical potential.

C. Fluctuation-induced pairing

Having discussed the unique energetics of pairing and spectral properties of the resulting superconductors in spin-polarized quasi-flat-bands with Dirac cones on a general level, we next study these aspects more explicitly by solving the superconducting self-consistency equations in the flat bands common to alternating-twist graphene systems. We will start with pairing induced by fluctuations of a nearby symmetry-broken phase. To this end, we will couple the low-energy electrons introduced in Eq. (1) to a collective bosonic field $\phi_j(q) = \phi_j^{\dagger}(-q)$ via

$$\mathcal{H}_{\phi} = \sum_{\boldsymbol{k},\boldsymbol{q},i} c_{\boldsymbol{k}+\boldsymbol{q},\alpha,\eta}^{\dagger} \lambda_{\alpha,\eta;\alpha',\eta'}^{j} c_{\boldsymbol{k},\alpha',\eta'} \phi_{j}(\boldsymbol{q}), \qquad (4)$$

where the Hermitian matrices λ^{j} capture the nature of the correlated insulating phase. Both for twisted bi-[9] and trilayer graphene [14, 15, 29], the stable phases emerging out of the $U(4) \times U(4)$ [9] manifold in the chiralflat (decoupled) limit are natural candidates. Integrating out the bosonic modes, we obtain an effective electronic interaction which in the for superconductivity relevant intervalley Cooper channel reads as

$$\mathcal{H}_{\text{int}}^{\phi} = -\sum_{\mathbf{k},\mathbf{k}'} \chi_{\mathbf{k}-\mathbf{k}'} \mathcal{V}_{(\eta,\alpha,\beta),(\eta',\alpha',\beta')}$$

$$\times c_{-\mathbf{k},\beta,-\eta}^{\dagger} c_{\mathbf{k},\alpha,\eta}^{\dagger} c_{\mathbf{k}',\alpha',\eta'}^{} c_{-\mathbf{k}',\beta',-\eta'}^{},$$

$$(5)$$

with vertex

$$\mathcal{V}_{(\eta,\alpha,\beta),(\eta',\alpha',\beta')} = t_{\phi} \sum_{j} [\lambda_{\beta,\eta;\beta',\eta'}^{j}]^* \lambda_{\alpha,\eta;\alpha',\eta'}^{j}, \quad (6)$$

 $t_{\phi} = \pm 1$ encoding whether the order parameter is even or odd under time-reversal, $\Theta \phi_j(\mathbf{q})\Theta^{\dagger} = t_{\phi}\phi_j(\mathbf{q})$, and $\chi_{\mathbf{q}} > 0$ denoting the (static) susceptibility of ϕ_j .

Before discussing numerical results for the full model, we first focus on perfectly flat bands. In this limit, one can show that the leading superconducting instability within mean-field theory is given by the largest eigenvalue of $\mathcal V$ in Eq. (6) viewed as a matrix in the multi-index (η, α, β) . Furthermore, if there is an anti-symmetric, valley-off-diagonal matrix D obeying

$$[D\eta_x, \lambda^j]_{-t_\phi} \equiv D\eta_x \lambda^j - t_\phi \lambda^j D\eta_x = 0, \tag{7}$$

the associated leading superconducting order parameter in Eq. (1) is given by $(\Delta_{\mathbf{k},\eta})_{\alpha,\alpha'} = \delta_{\mathbf{k}}(D\eta_x)_{\alpha,\eta;\alpha'\eta}$ with $\delta_{\mathbf{k}} > 0$; here η_j denote Pauli matrices in valley space and the precise form of $\delta_{\mathbf{k}}$ is determined by $\chi(\mathbf{q})$.

D. T-IVC fluctuations

Motivated by recent experiments [7] providing direct evidence for time-reversal symmetric intervalley coherent (T-IVC) order, we start with T-IVC fluctuations as a pairing glue. In the $U(4) \times U(4)$ symmetric limit, the T-IVC state is associated with $\lambda^{j} = \sigma_{0}\eta_{j}$, j = x, y, within our conventions. Since $t_{\phi} = +1$, we are looking for $D\eta_x$ that commutes with λ^j . Interestingly, there is a unique anti-symmetric, valley-off-diagonal matrix $D \propto \sigma_y \eta_x$ with that property, implying that the leading pairing state has the form $\Delta_{{m k},\eta} = \sigma_y \delta_{{m k}}, \ \delta_{{m k}} > 0.$ This is exactly the A_2 state in Table I, which, as discussed above, will have nodal lines at least in the vicinity of T_c when a finite band dispersion is taken into account. Intuitively, the fact that A_2 pairing is favored can be understood by noticing that the valleyoff-diagonal form of λ^{j} leads to an attractive interaction across the valleys, which penalizes the B_1 state which changes sign between the two valleys. In fact, it holds $\mathcal{V}_{(\eta,\alpha,\beta),(\eta',\alpha',\beta')} = (1 - \eta \eta') \sum_{\mu=0}^{3} (\sigma_{\mu}^{*})_{\alpha,\beta} (\sigma_{\mu})_{\alpha',\beta'}$ showing explicitly that it is repulsive (attractive) in the B_1 (A_2) channel.

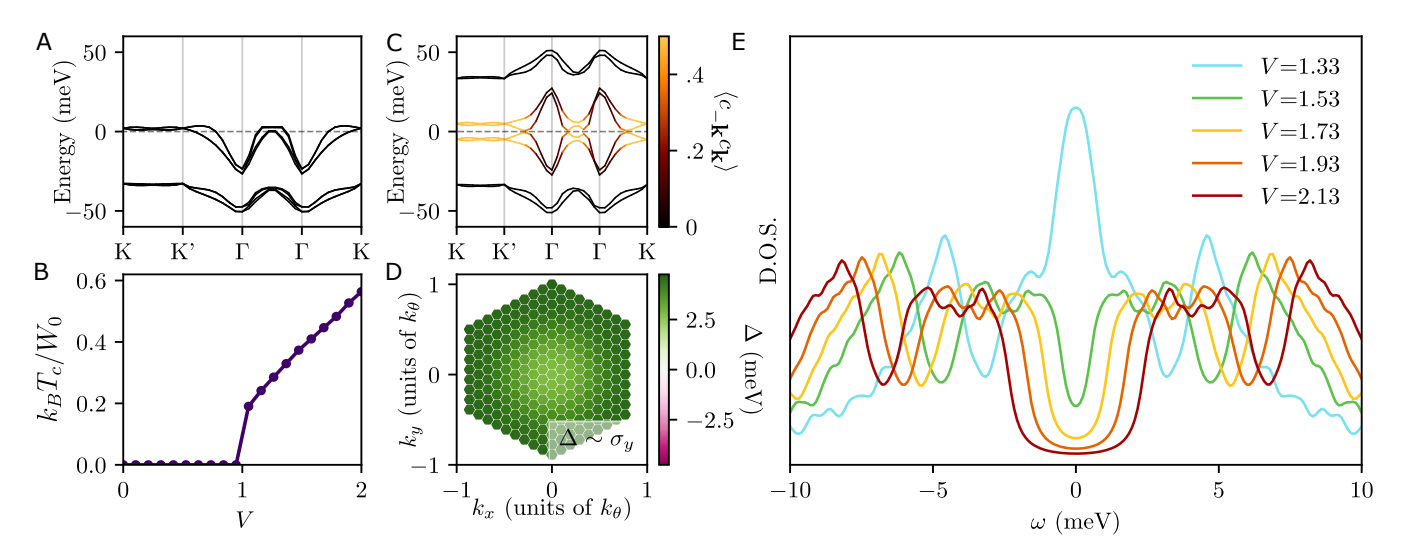


FIG. 2: Pairing mediated by T-IVC fluctuations. We show (a) the band structure of the normal state with spin polarization and (b) the critical temperature T_c (in units of the maximum band splitting $W_0 \simeq 9.4$ meV) as a function of coupling strength V measured in units of the critical coupling $V_{c,1} = 145 \text{ meV} \cdot \text{nm}^2$. The band structure (with color indicating the band-projected value of the anomalous correlator) of the A_2 state and its order parameter are shown in (c) and (d). The DOS of the T=0 superconductor for several different values of coupling strength V is plotted in (e). The DOS was computed as $DOS(\omega) = \sum_{\mathbf{k}} \delta\left(E_{\mathbf{k}} - \omega\right)$ where in practice we replace the δ function with Lorentzians with half width at half max 0.3 meV. The critical coupling $V_{c,2}$ where the nodal lines disappear is $V_{c,2} \simeq 1.4V_{c,1}$.

To go beyond the flat-band limit, we solve the superconducting mean-field equations numerically. We take the flat TBG bands from the continuum model [66] as the starting point. To capture the spin polarized normal state, we supplement it with Coulomb repulsion and a perform HF calculation (see Appendix A for details). As can be seen in the resulting band structure shown in Fig. 2(a) for filling fraction $\nu = 2$, this not only pushes one spin flavor below the Fermi level but also induces significant band renormalizations. For our subsequent study of superconducticity, we project onto the two bands at the Fermi level and associate them with the creation operators $c_{\mathbf{k},\alpha}$ in the interactions in Eqs. (4) and (5). In our numerical computations shown in Fig. 2, we choose $\chi(q) = \frac{1}{A_m} \frac{V}{\alpha^2 + |q|^2/k_\theta^2}$ where A_m is the real space area of a moiré unit cell, and take $\alpha = 0.2$ for concreteness, although we checked our main conclusion do not crucially depend on this form. In all of our numerics, we work at doping $\nu = 2.5$.

As expected, we indeed find that the A_2 state dominates in our numerical calculation, both right at the critical temperature T_c , obtained from the linearized gap equation, and at T=0 as we show by iteratively solving the full self-consistency equation (see Appendix C). One crucial effect of the finite dispersion and splitting between the bands is that a finite interaction strength, $V > V_{c,1}$, is required to stabilize the superconducting phase, as can be seen in the plot of T_c in Fig. 2(b). Superconductivity ceases to be a weak-coupling instability as the Bloch states $(\mathbf{k}, \alpha, \eta)$ and $(-\mathbf{k}, \alpha', -\eta)$ are not degenerate for

 $\alpha \neq \alpha'$, cutting off the logarithmic divergence known from BCS theory. The quasi-particle spectrum and order parameter of superconductivity from T=0 numerics is shown in Fig. 2(c,d). In accordance with our general discussion above, we observe that the order parameter only has finite components proportional to σ_y , which do not mix with the band-even contributions $\propto \sigma_{0,x,z}$ as a result of C_{2z} symmetry. Furthermore, it does not change sign as a function of k and, for sufficiently small V but still with $V > V_{c,1}$, the nodal lines in the superconducting spectrum persist all the way to T=0, while the nodal line is gapped out at low $T < T_c$ if $V > V_{c,2}$. The V-dependence of the superconducting gap can be more clearly seen in Fig. 2(e), where we show the DOS for the self-consistent solution at T=0. For large V, the superconductor becomes fully gapped at T=0, leading to a U-shaped DOS. With smaller V, the magnitude of the order parameter decreases and the superconductor eventually exhibits a nodal lines, as explained above. In the regime just before these nodal lines appear, the increased DOS near the Fermi level leads to a V-shaped DOS, roughly when the order parameter and the maximal band splitting are comparable. This behavior of the DOS with V offers another natural explanation for the U-shaped tunneling conductance measurements near $\nu = 2$ and V-shaped tunneling conductance measurements near $\nu = 3$ observed in TTG [49]; if we are considering T-IVC fluctuations of the insulator at $\nu = 2$, then it may be reasonable to expect the coupling to these fluctuations could grow weaker as we dope towards $\nu = 3$, in line with the experimentally

observed ν dependence. For small $V \gtrsim V_{c,1}$, a peak occurs at $\omega = 0$, which is due to the Van Hove singularity crossing the Fermi level. However, this feature is highly dependent on the structure of the normal state, which we approximate with HF corrections, and may not be universal or occur at smaller values of V.

E. Electron-phonon coupling

To illustrate that the off-diagonal A_2 state is more generally favored beyond just T-IVC fluctuations, we next discuss electron-phonon coupling, which is frequently considered as a plausible pairing mechanism for twisted moiré systems [33, 35–39]. Similar to Ref. 35, we use that the optical A_2 , B_1 , and E_2 phonon modes are known [68] to dominate the electron-phonon coupling in single-layer graphene. As these are optical phonons, we further assume that the impact of the interlayer coupling on the phonons can be neglected and arrive at

$$\mathcal{H}_{EP} = \int d\mathbf{r} \, \psi_{\ell,s}^{\dagger}(\mathbf{r}) [g_{A_1} \Lambda_{A_1} u_{A_1,\mu}(\mathbf{r})$$
 (8)

$$+\,g_{B_1}\Lambda_{B_1}u_{B_1,\mu}(\bm{r})+g_{E_2}\bm{\Lambda}_{E_2}\cdot\bm{u}_{E_2,\mu}(\bm{r})](\bm{v}_{\mu})_\ell\psi_{\ell,s}(\bm{r})$$

for the electron-phonon coupling. Symmetry dictates that the vertices Λ_g are given by $\Lambda_{A_1} = \eta_x \rho_x$, $\Lambda_{B_1} = \eta_y \rho_x$, and $\Lambda_{E_2} = (\eta_z \rho_y, -\rho_x)$; for this reason, we refer to the A_1 , B_1 (E_2) phonons as intervalley (intravalley) phonon modes in the following. The coupling constants obey $g_{A_1} = g_{B_1} \simeq g_{E_2}$ [68]. The associated displacement operators in Eq. (8) can be expressed in the usual way in terms of canonical bosons, $b_{q,\alpha,\mu,q}$,

$$(u_{g,\mu}(\mathbf{r}))_j = \sum_{\mathbf{q}} \frac{b_{g,j,\mu,\mathbf{q}} e^{i\mathbf{q}\cdot\mathbf{r}} + \text{H.c.}}{\sqrt{2NM\omega_g(\mathbf{q})}},$$
 (9)

where j refers to the two components for the E_2 phonon (is idle for A_1 , B_1), M is the carbon mass, and $\omega_q(\mathbf{q})$ is the phonon dispersion, characterizing the phononic part of the Hamiltonian, $\mathcal{H}_P = \sum_{\boldsymbol{q}} \omega_g(\boldsymbol{q}) b^{\dagger}_{g,j,\mu,\boldsymbol{q}} b_{g,j,\mu,\boldsymbol{q}}$. Finally, \boldsymbol{v}_{μ} in Eq. (8) encodes the (pseudo)layer-structure of the phonon modes. In case of TBG, $\ell = 1, 2$ refers to the physical graphene layer and one can, in principle, choose any orthonormal basis; we will find it convenient to use the layer-exchange even and odd states, $u_{\pm} = (1, \pm 1)^T / \sqrt{2}$. For TTG, the situation is more involved due to the projection into the mirror-even space: starting from uncoupled optical A_1 , B_1 , and E_2 phonons in the three layers of TTG, we can decompose each of these modes into two mirror-even and one mirrorodd modes; upon projection into the mirror-even electronic sector, the last type of modes vanishes and we are left with the two mirror-even modes. Their coupling is of the form of Eq. (8) with $v_{+}=(1,1)^{T}/\sqrt{3}$ and $\mathbf{v}_{-} = (1, -2)^{T}/\sqrt{6}$. While we only show numerical results in the following for the case of TBG, we expect our

arguments about which phonons are attractive in which pairing channels will hold for both systems.

We project \mathcal{H}_{EP} onto the two flat bands ($\alpha = \pm$) in each valley η of the spin polarized continuum-model flat-bands, leading to a coupling term similar to Eq. (4) with momentum-dependent coupling matrices, $\lambda^j \to \lambda_{k,k'}^{g,j,\mu}$. Neglecting the momentum dependence in the phonon frequencies and retardation effects, the resulting electron-electron interaction in the inter-valley Cooper channel obtained by integrating out the phonons reads as

$$\mathcal{H}_{\text{int}}^{C} = -\sum_{\mathbf{k},\mathbf{k}'} V_{g} [\lambda_{\mathbf{k},\beta,\eta;\mathbf{k}',\beta',\eta'}^{g,j,\mu}]^{*} \lambda_{\mathbf{k},\alpha,\eta;\mathbf{k}',\alpha',\eta'}^{g,j,\mu}$$

$$\times c_{-\mathbf{k},\beta,-\eta}^{\dagger} c_{\mathbf{k},\alpha,\eta}^{\dagger} c_{\mathbf{k}',\alpha',\eta'}^{\dagger} c_{-\mathbf{k}',\beta',-\eta'}^{\dagger}.$$

$$(10)$$

Here, $V_g = g_g^2/(2N\omega_g^2) > 0$ are the effective coupling constants of the three different phonon modes $g = A_1, B_1, E_2$. Based on the estimated phonon frequencies of Ref. 68, we have $V_{A_1} = V_{B_1} \simeq 1.33 V_{E_2}$. From Eq. (10), it is clear that the induced interaction would be always completely attractive if we focused on intra-band pairing, $\alpha = \alpha' = \beta = \beta'$, which in spinful systems generically favors the trivial pairing channel [51, 52]. In our case, the combination of two energetically close bands and the trivial pairing being purely band-off-diagonal, thus, leads to the competition between different superconductors, even with electron-phonon coupling alone.

To demonstrate this, we study intra-valley pairing within the mean-field approximation and parametrize the relative strength of the different phonon modes with an angle variable $\theta_{\rm ph}$ according to $V_{A_1} = V_{B_1} = V_0 \cos \theta_{\rm ph}$, $V_{E_2} = V_0 \sin \theta_{\rm ph}$. Investigating the matrix elements $\lambda_{k,k'}^{g,j,\mu}$, we notice that they almost vanish for the layer-odd intervalley (A_1, B_1) phonons, which can be understood as a consequence of chiral and particle-hole symmetry. The situation is the reverse for the intravalley (E_2) phonons, where the layer-even matrix elements are numerically small and the layer-odd matrix elements dominate. We therefore focus on layer-even (odd) intervalley (intravalley) phonon couplings.

The results of the mean-field calculation are summarized in Fig. 3. We see that the A_2 pairing state is favored by the intervalley phonons $(\theta_{\rm ph}=0)$ inspite of its band-off-diagonal nature leading to a suppressed gap [see Fig. 3(a)]. This is natural as these phonons mediate an attractive interaction between the two valleys which disfavors the B_1 state, similar to T-IVC fluctuations. In fact, focusing on the leading, momentum independent term, $\lambda_{\mathbf{k},\mathbf{k}'}^{g,+} \to \lambda^{g,+}$, $g=A_1,B_1$, symmetry dictates $\lambda^{A_1,+} \propto \sigma_0 \eta_1$ and $\lambda^{B_1,+} \propto \sigma_0 \eta_2$ in the chiral limit. This maps the problem exactly to that of T-IVC fluctuations, immediately explaining why the order parameter has a fixed sign in Fig. 3(b). As $\theta_{\rm ph}$ is increased, the B_1 state is favored as can be seen in Fig. 3(c). This is expected since the intravalley E_2 phonon mediates an

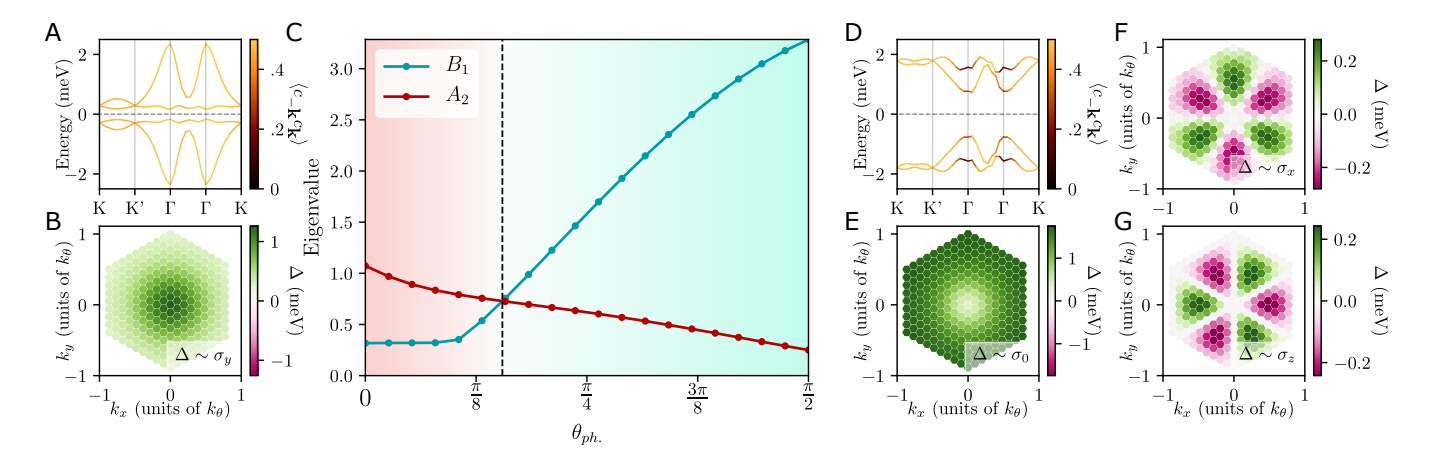


FIG. 3: Pairing from electron-phonon coupling. We show (a) the band structure and (b) the self consistent order parameter of the A_2 pairing for $\theta_{\rm ph}=0$ and T=0. The eigenvalues corresponding to the A_2 and B_1 pairings in the linearized gap equation at $T=5\,\rm K$, which is close to their T_c , are shown in (c) as a function of $\theta_{\rm ph}$. We show an example of the band structure (d) of the B_1 pairing and its order parameter (e,f,g). In accordance with symmetry, the A_2 (B_1) state only has order-parameter components $\propto \sigma_y$ ($\propto \sigma_{0,x,z}$). We took $\nu=2.5$ and $V_0=600~\rm meV\cdot(nm)^2$ with a continuum model bandwidth $\simeq 2~\rm meV$. We point out that if A_1 phonons are dominant, as suggested by recent experimental work [61] and past theoretical study in mono-layer graphene [67], we would expect our A_2 pairing to dominate assuming the pairing potential is sufficiently large.

attractive interaction within each valley such that the energy gain due to the enhanced gap [Fig. 3(d)], associated with the band-diagonal matrix elements of the B_1 state, will overcompensate the energetic loss due to the sign change of B_1 's order parameter between the two valleys. This picture is consistent with the dominance and non-sign-changing nature of the band-diagonal components of the B_1 state, see Fig. 3(e-g). Finally, this behavior can also be understood by applying the commutator criterion in Eq. (7) in the microscopic sublattice basis.

This shows that, as opposed to the conventional scenario [51, 52], there are two possible leading superconducting states and the superconducting pairing state does not transform trivially under the symmetries of the system even when phonons alone provide the pairing glue. Besides this conceptually important point, we note, however, that the resulting pairing strength based on phonons alone is likely not enough to explain superconductivity in TBG and TTG, as we discuss in more detail below. For comparison, estimating V_0 based on Ref. 68, we get $60-70 \text{ meV} \cdot (\text{nm})^2$, which is much smaller than the value we needed to stabilize superconductivity with a critical temperature of a few K for the normalstate band structure in Fig. 2(a). As such, additional particle-hole fluctuations, such as those of T-IVC order, might also be important for pairing.

F. Other particle-hole fluctuations

Finally, we discuss pairing induced by fluctuations of other particle-hole instabilities. In Table II, we list the resulting leading superconductors taking λ^j in Eq. (4) to be

TABLE II: Leading superconducting states in the flat-band limit, following from Eq. (7), for pairing mediated by fluctuations of the indicated orders, defined by using λ^j in Eq. (4). Here $\delta_k > 0$ and states separated by commas are degenerate. The couplings in the microscopic basis, used in Fig. 4 for the respective orders, are listed under $\bar{\lambda}^j$.

Fluctuating Order			Leading Superconductor	
type	λ^{j}	$ar{\lambda}^j$	$\Delta_{m{k},\eta}$	IR
T-IVC	$\sigma_0\eta_{x,y}$	$\rho_x \eta_{x,y}$	$\sigma_y \delta_{m k}$	A_2
K-IVC	$\sigma_y \eta_{x,y}$	$ ho_y \eta_{x,y}$	$\sigma_0\eta\delta_{m k}$	B_1
SLP_{+}	$\sigma_y \eta_z$	$ ho_z\eta_0$	$\sigma_y \delta_{m k}, \ \sigma_0 \eta \delta_{m k}$	A_2, B_1
SLP	$\sigma_y \eta_0$	$ ho_z\eta_z$	$\sigma_x \eta \delta_{\mathbf{k}}, \ \sigma_z \eta \delta_{\mathbf{k}}$	B_2, B_1

any of the different strong-coupling candidate order parameters [9]. To analyze how sensitive these conclusions are to the precise (momentum-independent) form of λ^{j} . we also perform numerics taking the expressions listed as $\bar{\lambda}^j$ in Table II; these are then projected to the flat bands, leading to momentum-dependent coupling vertices, cf. Eq. (10). The results are shown in Fig. 4, where we use the angle $\theta_{\text{fluc.}}$ to tune the relative strength between T-IVC and any of the other type of fluctuationinduced interactions by multiplying the T-IVC pairing potential with $\cos(\theta_{\text{fluc.}})$ and the other fluctuation potential with $\sin(\theta_{\text{fluc.}})$ such that $\theta_{\text{fluc.}} = 0$ corresponds to purely T-IVC fluctuations. In our microscopic numerics, we have taken a potential form $\chi(q) = \frac{1}{A_m} \frac{V}{\alpha^2 + |q|^2/k_a^2}$ again with $\alpha = 0.2$ and with $V = 2100 \text{ meV} \cdot (\text{nm})^2$. We chose the value of V such that the transitions between the

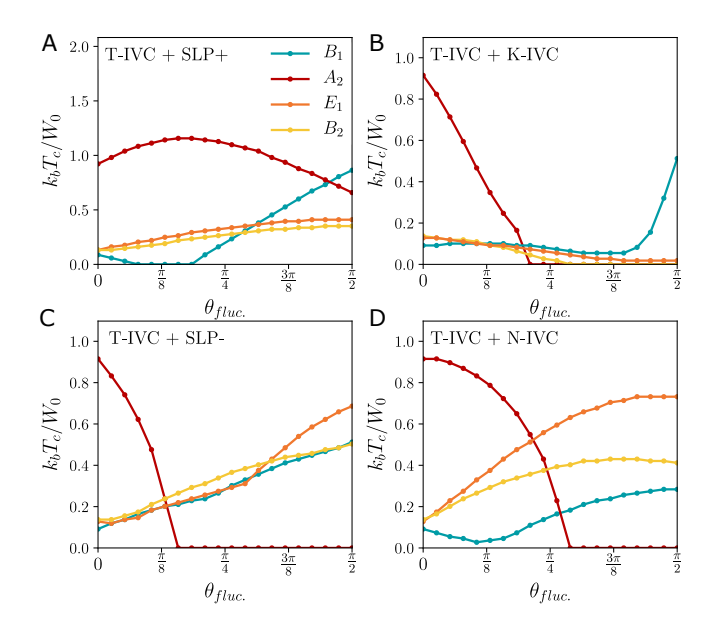


FIG. 4: Pairing for different particle-hole fluctuations. Similar to Fig. 3(c), we show T_c of the leading pairing states, where $\theta_{\rm fluc}$ tunes the relative strength between T-IVC-induced interactions ($\propto \cos \theta_{\rm fluc}$) and interactions ($\propto \sin \theta_{\rm fluc}$) coming from fluctuations of (a) SLP⁺, (b) K-IVC, (c) SLP⁻, and (d) N-IVC fluctuations.

different pairing states are clearly visible in Fig. 4 when varying $\theta_{\text{fluc.}}$. In accordance with the strong-coupling form, SLP⁺ fluctuations further stabilize the A_2 superconductor, see Fig. 4(a). As such, the band-diagonal B_1 superconducting channel, where SLP⁺ fluctuations are also attractive, can become the leading channel (favored over A_2 as a result of the finite bandwidth) only very close to $\theta_{\text{fluc.}} = \pi/2$. K-IVC fluctuations, however, are repulsive for A_2 pairing and favor the B_1 state more strongly. As the B_1 state is generically fully gapped, K-IVC fluctuations providing the dominant pairing glue is less natural given the V-shaped tunneling data of Ref. 49.

So far, the strong-coupling (λ^j) and sublattice $(\bar{\lambda}^j)$ form of the couplings in Table II lead to the same conclusions. This is different for SLP⁻ fluctuations [Fig. 4(d)], where the projection-induced momentum-dependence in the band basis can stabilize the E_1 superconductor. This can be understood by applying Eq. (7) in the sublattice basis. We also find the E_1 state when fluctuations of the layer-odd nematic intervalley-coherent state (N-IVC) of Ref. 62 dominate. While the N-IVC state, characterized by a matrix order parameter $\lambda^{(j,j')} = (\eta_x, \eta_y)_j(\rho_0, \rho_z)_{j'}$, does not appear in the limit of strong Coulomb repulsion, we include it here given recent experiments [7]. Examples of the E_1 nematic and B_2 order parameter which emerge for SLP- fluctuations or N-IVC fluctuations are shown in App. D. We point out the nematic E_1 pairing is also an interesting candidate given that despite having nonzero pairing in the σ_0 , σ_x , σ_z channels, it may still be

nodal as long as the σ_x components do not gap out the nodes in the band-diagonal parts.

III. DISCUSSION

Taken together, we see that the proposed band-offdiagonal A_2 superconductor is an especially attractive candidate for TBG and TTG: first, it can lead to both V-shaped or U-shaped DOS, see Fig. 2(e), depending on the coupling strength V. Because V might vary from sample to sample and within a sample (e.g., decrease upon doping further away from the insulator), this can naturally explain the tunneling data of [48, 49]. We emphasize however that at least at the level of our meanfield numerics, we only expect a V-shape in the regime where the superconducting pairing is of the order of the bandwidth; this is the regime, where although the pairing is finite and can be quite large, the gap in the BdG spectrum is either just closing or very small relative to the pairing. Increasing the pairing further will lead to an evolution from V to U shaped while decreasing the pairing will eventually lead to a nodal Fermi surface and presumably a peak at zero energy in the DOS. Second, A_2 is the unique pairing state that is favored by fluctuations of two out of the four strong-coupling-candidates we consider for the correlated insulator, see Fig. 4(a-c). What is more, this includes the T-IVC state, signatures of which are observed in recent experiments [7]. Finally, it is also favored by the likely dominant [61, 67] optical intervalley phonon modes. While in our numerics, we have assumed couplings generically much larger than estimated optical phonon couplings, we emphasize that the minimum attractive coupling needed to stabilize a purely band off diagonal state depends on the energy splitting between the two flat bands; if the bands of our normal state are closer to degenerate, irrespective of the total bandwidth, the needed coupling to stabilize the A_2 pairing in mean-field will decrease (as will T_c). At the very least, we have shown that phonons do not generically disfavor A_2 pairing and, in fact, in the additional presence of particle-hole fluctuations can further tip the balance in favor of it.

The other band-off-diagonal superconductor we identify transforms under the IR E_2 , i.e., can be thought of as a d-wave state. Its spectral properties also agree well with experiment as the chiral configurations, $E_2(1,i)$, which is favored within mean-field theory over a nematic E_2 state, can also have nodal regions, depending on filling. As can be seen in Fig. 1(d), this can lead to a transition from gapped to nodal when increasing the electron filling starting at $\nu \simeq 2$. However, as opposed to the A_2 state, E_2 does not naturally appear as leading instability when considering optical phonons or fluctuations of any of the strong-coupling order parameters of the correlated

insulator. While this makes it energetically less natural than A_2 , we cannot exclude it since its phenomenology agrees well with experiment and since the precise form of the coupling of the dominant low-energy collective excitations are not known—significant momentum dependencies beyond λ^j and $\bar{\lambda}^j$ in Table II could stabilize E_2 pairing as well. We also find in our numerics a nematic E_1 state which may be preferred over its chiral version in the presence of sufficient strain or due to fluctuation corrections [27, 53–55]. We find the E_1 state is the leading instability of nematic IVC fluctuations and SLP- fluctuations, and is a subleading instability of T-IVC fluctuations. The E_1 state is interesting in its own right, as it can also be nodal.

For the future, it will be interesting to go beyond mean-field and analyze the competition of our band-off-diagonal states with odd-frequency pairing, which we study in a follow-up work [69]. On a more general level, our work shows that the observation of nodal pairing in twisted graphene systems does not immediately exclude a chiral superconducting state nor an entirely electron-phonon-based pairing mechanism. It illustrates that a

microscopic understanding of the superconducting states in graphene moiré systems requires taking into account their intrinsically multi-band nature.

Note added. Just before posting our work, Ref. 70 appeared online, which discusses pairing induced by A_1 phonons in spinful TBG bands.

ACKNOWLEDGMENTS

M.S.S. acknowledges funding by the European Union (ERC-2021-STG, Project 101040651—SuperCorr). Views and opinions expressed are however those of the authors only and do not necessarily reflect those of the European Union or the European Research Council Executive Agency. Neither the European Union nor the granting authority can be held responsible for them. M.C. and S.S. acknowledge funding by U.S. National Science Foundation grant No. DMR-2002850. M.S.S. thanks B. Putzer for discussions. M.C. thanks P. Ledwith and J. Dong for helpful discussions.

- [1] E. Y. Andrei and A. H. MacDonald, "Graphene bilayers with a twist," Nature Materials 19, 1265 (2020).
- [2] L. Balents, C. R. Dean, D. K. Efetov, and A. F. Young, "Superconductivity and strong correlations in moiré flat bands," Nature Physics 16, 725 (2020).
- [3] Y. Cao, V. Fatemi, A. Demir, S. Fang, S. L. Tomarken, J. Y. Luo, J. D. Sanchez-Yamagishi, K. Watanabe, T. Taniguchi, E. Kaxiras, R. C. Ashoori, and P. Jarillo-Herrero, "Correlated insulator behaviour at half-filling in magic-angle graphene superlattices," Nature 556, 80 (2018).
- [4] X. Lu, P. Stepanov, W. Yang, M. Xie, M. A. Aamir, I. Das, C. Urgell, K. Watanabe, T. Taniguchi, G. Zhang, A. Bachtold, A. H. MacDonald, and D. K. Efetov, "Superconductors, orbital magnets and correlated states in magic-angle bilayer graphene," Nature 574, 653 (2019).
- [5] A. L. Sharpe, E. J. Fox, A. W. Barnard, J. Finney, K. Watanabe, T. Taniguchi, M. A. Kastner, and D. Goldhaber-Gordon, "Emergent ferromagnetism near three-quarters filling in twisted bilayer graphene," Science 365, 605 (2019).
- [6] K. P. Nuckolls, M. Oh, D. Wong, B. Lian, K. Watanabe, T. Taniguchi, B. A. Bernevig, and A. Yazdani, "Strongly correlated chern insulators in magic-angle twisted bilayer graphene," Nature 588, 610 (2020).
- [7] K. P. Nuckolls, R. L. Lee, M. Oh, D. Wong, T. Soejima, J. P. Hong, D. Călugăru, J. Herzog-Arbeitman, B. A. Bernevig, K. Watanabe, T. Taniguchi, N. Regnault, M. P. Zaletel, and A. Yazdani, "Quantum textures of the many-body wavefunctions in magic-angle graphene," (2023).
- [8] J. Kang and O. Vafek, "Strong Coupling Phases of Partially Filled Twisted Bilayer Graphene Narrow Bands,"

- Phys. Rev. Lett. **122**, 246401 (2019), arXiv:1810.08642 [cond-mat.str-el].
- [9] N. Bultinck, E. Khalaf, S. Liu, S. Chatterjee, A. Vishwanath, and M. P. Zaletel, "Ground State and Hidden Symmetry of Magic-Angle Graphene at Even Integer Filling," Phys. Rev. X 10, 031034 (2020), arXiv:1911.02045 [cond-mat.str-el].
- [10] T. Soejima, D. E. Parker, N. Bultinck, J. Hauschild, and M. P. Zaletel, "Efficient simulation of moiré materials using the density matrix renormalization group," Phys. Rev. B 102 (2020).
- [11] F. Xie, A. Cowsik, Z.-D. Song, B. Lian, B. A. Bernevig, and N. Regnault, "Twisted bilayer graphene. VI. an exact diagonalization study at nonzero integer filling," Phys. Rev. B 103 (2021), 10.1103/physrevb.103.205416.
- [12] Y. Kwan, G. Wagner, T. Soejima, M. Zaletel, S. Simon, S. Parameswaran, and N. Bultinck, "Kekulé spiral order at all nonzero integer fillings in twisted bilayer graphene," Phys. Rev. X 11 (2021), 10.1103/physrevx.11.041063.
- [13] M. Christos, S. Sachdev, and M. S. Scheurer, "Correlated Insulators, Semimetals, and Superconductivity in Twisted Trilayer Graphene," Phys. Rev. X 12, 021018 (2022), arXiv:2106.02063 [cond-mat.str-el].
- [14] F. Xie, N. Regnault, D. Că lugăru, B. A. Bernevig, and B. Lian, "Twisted symmetric trilayer graphene. II. projected hartree-fock study," Phys. Rev. B 104 (2021), 10.1103/physrevb.104.115167.
- [15] P. J. Ledwith, E. Khalaf, Z. Zhu, S. Carr, E. Kaxiras, and A. Vishwanath, "Tb or not tb? contrasting properties of twisted bilayer graphene and the alternating twist n-layer structures $(n=3,4,5,\ldots)$," (2021), arXiv:2111.11060 [cond-mat.str-el].
- [16] G. Wagner, Y. H. Kwan, N. Bultinck, S. H. Simon, and

- S. Parameswaran, "Global phase diagram of the normal state of twisted bilayer graphene," Phys. Rev. Lett. **128** (2022), 10.1103/physrevlett.128.156401.
- [17] T. Wang, D. E. Parker, T. Soejima, J. Hauschild, S. Anand, N. Bultinck, and M. P. Zaletel, "Kekulé spiral order in magic-angle graphene: a density matrix renormalization group study," (2022), arXiv:2211.02693 [cond-mat.str-el].
- [18] Y. H. Kwan, G. Wagner, N. Bultinck, S. H. Simon, E. Berg, and S. A. Parameswaran, "Electron-phonon coupling and competing kekulé orders in twisted bilayer graphene," (2023), arXiv:2303.13602 [cond-mat.str-el].
- [19] D. Wong, K. P. Nuckolls, M. Oh, B. Lian, Y. Xie, S. Jeon, K. Watanabe, T. Taniguchi, B. A. Bernevig, and A. Yazdani, "Cascade of electronic transitions in magic-angle twisted bilayer graphene," Nature 582, 198 (2020).
- [20] U. Zondiner, A. Rozen, D. Rodan-Legrain, Y. Cao, R. Queiroz, T. Taniguchi, K. Watanabe, Y. Oreg, F. von Oppen, A. Stern, E. Berg, P. Jarillo-Herrero, and S. Ilani, "Cascade of phase transitions and dirac revivals in magic-angle graphene," Nature 582, 203 (2020).
- [21] J. M. Park, Y. Cao, K. Watanabe, T. Taniguchi, and P. Jarillo-Herrero, "Tunable strongly coupled superconductivity in magic-angle twisted trilayer graphene," Nature 590, 249 (2021).
- [22] Z. Hao, A. M. Zimmerman, P. Ledwith, E. Khalaf, D. H. Najafabadi, K. Watanabe, T. Taniguchi, A. Vishwanath, and P. Kim, "Electric field-tunable superconductivity in alternating-twist magic-angle trilayer graphene," Science 371, 1133 (2021).
- [23] J.-X. Lin, P. Siriviboon, H. D. Scammell, S. Liu, D. Rhodes, K. Watanabe, T. Taniguchi, J. Hone, M. S. Scheurer, and J. I. A. Li, "Zero-field superconducting diode effect in small-twist-angle trilayer graphene," Nature Physics 18, 1221 (2022).
- [24] E. Morissette, J.-X. Lin, D. Sun, L. Zhang, S. Liu, D. Rhodes, K. Watanabe, T. Taniguchi, J. Hone, J. Pollanen, M. S. Scheurer, M. Lilly, A. Mounce, and J. I. A. Li, "Electron spin resonance and collective excitations in magic-angle twisted bilayer graphene," (2022), arXiv:2206.08354 [cond-mat].
- [25] Y. Cao, J. M. Park, K. Watanabe, T. Taniguchi, and P. Jarillo-Herrero, "Pauli-limit violation and re-entrant superconductivity in moirégraphene," Nature 595, 526 (2021).
- [26] R. Ojajärvi, T. Hyart, M. A. Silaev, and T. T. Heikkilä, "Competition of electron-phonon mediated superconductivity and stoner magnetism on a flat band," Phys. Rev. B 98, 054515 (2018).
- [27] M. S. Scheurer and R. Samajdar, "Pairing in graphene-based moiré superlattices," Phys. Rev. Research 2, 033062 (2020).
- [28] E. Lake, A. S. Patri, and T. Senthil, "Pairing symmetry of twisted bilayer graphene: A phenomenological synthesis," Phys. Rev. B 106 (2022), 10.1103/physrevb.106.104506.
- [29] M. Christos, S. Sachdev, and M. S. Scheurer, "Super-conductivity, correlated insulators, and Wess-Zumino-Witten terms in twisted bilayer graphene," Proceedings of the National Academy of Science 117, 29543 (2020), the T-IVC state was denoted IVC+ in this paper,

- arXiv:2007.00007 [cond-mat.str-el].
- [30] E. Khalaf, S. Chatterjee, N. Bultinck, M. P. Zaletel, and A. Vishwanath, "Charged skyrmions and topological origin of superconductivity in magic-angle graphene," Science Advances 7 (2021), 10.1126/sciadv.abf5299.
- [31] E. Khalaf, P. Ledwith, and A. Vishwanath, "Symmetry constraints on superconductivity in twisted bilayer graphene: Fractional vortices, 4e condensates, or nonunitary pairing," Phys. Rev. B 105, 224508 (2022).
- [32] H. D. Scammell, J. I. A. Li, and M. S. Scheurer, "Theory of zero-field superconducting diode effect in twisted trilayer graphene," 2D Materials 9, 025027 (2022).
- [33] G. Shavit, E. Berg, A. Stern, and Y. Oreg, "Theory of correlated insulators and superconductivity in twisted bilayer graphene," Phys. Rev. Lett. **127**, 247703 (2021).
- [34] V. Crépel, T. Cea, L. Fu, and F. Guinea, "Unconventional superconductivity due to interband polarization," Phys. Rev. B 105, 094506 (2022).
- [35] F. Wu, A. H. MacDonald, and I. Martin, "Theory of phonon-mediated superconductivity in twisted bilayer graphene," Phys. Rev. Lett. 121, 257001 (2018).
- [36] B. Lian, Z. Wang, and B. A. Bernevig, "Twisted bilayer graphene: A phonon-driven superconductor," Phys. Rev. Lett. 122, 257002 (2019).
- [37] C. Lewandowski, D. Chowdhury, and J. Ruhman, "Pairing in magic-angle twisted bilayer graphene: Role of phonon and plasmon umklapp," Phys. Rev. B 103, 235401 (2021).
- [38] C. Lewandowski, S. Nadj-Perge, and D. Chowdhury, "Does filling-dependent band renormalization aid pairing in twisted bilayer graphene?" npj Quantum Materials 6, 82 (2021).
- [39] J. Yu, M. Xie, F. Wu, and S. Das Sarma, "Euler Obstructed Cooper Pairing in Twisted Bilayer Graphene: Nematic Nodal Superconductivity and Bounded Superfluid Weight," arXiv e-prints (2022), 10.48550/arXiv.2202.02353, arXiv:2202.02353 [cond-mat.supr-con].
- [40] V. o. T. Phong, P. A. Pantaleón, T. Cea, and F. Guinea, "Band structure and superconductivity in twisted trilayer graphene," Phys. Rev. B 104, L121116 (2021).
- [41] Y. Wang, J. Kang, and R. M. Fernandes, "Topological and nematic superconductivity mediated by ferro-SU(4) fluctuations in twisted bilayer graphene," Phys. Rev. B 103 (2021), 10.1103/physrevb.103.024506.
- [42] C. Huang, N. Wei, W. Qin, and A. H. MacDonald, "Pseudospin paramagnons and the superconducting dome in magic angle twisted bilayer graphene," Phys. Rev. Lett. 129, 187001 (2022).
- [43] A. Fischer, L. Klebl, C. Honerkamp, and D. M. Kennes, "Spin-fluctuation-induced pairing in twisted bilayer graphene," Phys. Rev. B **103**, L041103 (2021).
- [44] J. Herzog-Arbeitman, A. Chew, K.-E. Huhtinen, P. Törmä, and B. A. Bernevig, "Many-Body Superconductivity in Topological Flat Bands," arXiv e-prints (2022), arXiv:2209.00007 [cond-mat.str-el].
- [45] T. Cea and F. Guinea, "Coulomb interaction, phonons, and superconductivity in twisted bilayer graphene," Proceedings of the National Academy of Sciences 118 (2021), 10.1073/pnas.2107874118.
- [46] V. Kozii, M. P. Zaletel, and N. Bultinck, "Spin-triplet

- superconductivity from intervalley goldstone modes in magic-angle graphene," Phys. Rev. B 106 (2022), 10.1103/physrevb.106.235157.
- [47] Y.-Z. You and A. Vishwanath, "Superconductivity from valley fluctuations and approximate so(4) symmetry in a weak coupling theory of twisted bilayer graphene," npj Quantum Materials 4, 16 (2019).
- [48] M. Oh, K. P. Nuckolls, D. Wong, R. L. Lee, X. Liu, K. Watanabe, T. Taniguchi, and A. Yazdani, "Evidence for unconventional superconductivity in twisted bilayer graphene," Nature 600, 240 (2021).
- [49] H. Kim, Y. Choi, C. Lewandowski, A. Thomson, Y. Zhang, R. Polski, K. Watanabe, T. Taniguchi, J. Alicea, and S. Nadj-Perge, "Evidence for unconventional superconductivity in twisted trilayer graphene," Nature 606, 494 (2022).
- [50] P. P. Poduval and M. S. Scheurer, "Vestigial singlet pairing in a fluctuating magnetic triplet superconductor: Applications to graphene moiré systems," arXiv e-prints (2023), arXiv:2301.01344 [cond-mat.supr-con].
- [51] P. M. R. Brydon, S. Das Sarma, H.-Y. Hui, and J. D. Sau, "Odd-parity superconductivity from phononmediated pairing: Application to Cu_xBi₂Se₃," Phys. Rev. B 90, 184512 (2014).
- [52] M. S. Scheurer, "Mechanism, time-reversal symmetry, and topology of superconductivity in noncentrosymmetric systems," Phys. Rev. B 93, 174509 (2016).
- [53] P. W. Anderson and W. F. Brinkman, "Anisotropic superfluidity in ³He: A possible interpretation of its stability as a spin-fluctuation effect," Phys. Rev. Lett. 30, 1108 (1973).
- [54] V. Kozii, H. Isobe, J. W. F. Venderbos, and L. Fu, "Nematic superconductivity stabilized by density wave fluctuations: Possible application to twisted bilayer graphene," Phys. Rev. B 99, 144507 (2019).
- [55] V. Gali and R. M. Fernandes, "Role of electromagnetic gauge-field fluctuations in the selection between chiral and nematic superconductivity," Phys. Rev. B 106, 094509 (2022).
- [56] P. M. R. Brydon, D. F. Agterberg, H. Menke, and C. Timm, "Bogoliubov Fermi surfaces: General theory, magnetic order, and topology," Phys. Rev. B 98 (2018).
- [57] D. Agterberg, P. Brydon, and C. Timm, "Bogoliubov Fermi Surfaces in Superconductors with Broken Time-Reversal Symmetry," Phys. Rev. Lett. 118 (2017).
- [58] N. Read and S. Sachdev, "Spin-Peierls, valence-bond solid, and Néel ground states of low-dimensional quantum antiferromagnets," Phys. Rev. B 42, 4568 (1990), Appendix B.

- [59] J. Lee and S. Sachdev, "Wess-Zumino-Witten Terms in Graphene Landau Levels," Phys. Rev. Lett. **114**, 226801 (2015), arXiv:1411.5684 [cond-mat.str-el].
- [60] X. Liu, G. Farahi, C.-L. Chiu, Z. Papic, K. Watanabe, T. Taniguchi, M. P. Zaletel, and A. Yazdani, "Visualizing broken symmetry and topological defects in a quantum Hall ferromagnet," Science 375, 321 (2022), arXiv:2109.11555 [cond-mat.mes-hall].
- [61] C. Chen, K. P. Nuckolls, S. Ding, W. Miao, D. Wong, M. Oh, R. L. Lee, S. He, C. Peng, D. Pei, Y. Li, S. Zhang, J. Liu, Z. Liu, C. Jozwiak, A. Bostwick, E. Rotenberg, C. Li, X. Han, D. Pan, X. Dai, C. Liu, B. A. Bernevig, Y. Wang, A. Yazdani, and Y. Chen, "Strong inter-valley electron-phonon coupling in magic-angle twisted bilayer graphene," (2023), arXiv:2303.14903 [cond-mat.meshall].
- [62] R. Samajdar, M. S. Scheurer, S. Turkel, C. Rubio-Verdú, A. N. Pasupathy, J. W. F. Venderbos, and R. M. Fernandes, "Electric-field-tunable electronic nematic order in twisted double-bilayer graphene," 2D Materials 8, 034005 (2021).
- [63] L. Zou, H. C. Po, A. Vishwanath, and T. Senthil, "Band structure of twisted bilayer graphene: Emergent symmetries, commensurate approximants, and wannier obstructions," Phys. Rev. B 98, 085435 (2018).
- [64] M. S. Scheurer, D. F. Agterberg, and J. Schmalian, "Selection rules for cooper pairing in two-dimensional interfaces and sheets," npj Quantum Materials 2, 9 (2017).
- [65] S. Yip and A. Garg, "Superconducting states of reduced symmetry: General order parameters and physical implications," Phys. Rev. B 48, 3304 (1993).
- [66] R. Bistritzer and A. H. MacDonald, "Moiré bands in twisted double-layer graphene," Proceedings of the National Academy of Sciences 108, 12233 (2011).
- [67] D. M. Basko and I. L. Aleiner, "Interplay of Coulomb and electron-phonon interactions in graphene," Phys. Rev. B 77 (2008), 10.1103/physrevb.77.041409.
- [68] D. M. Basko and I. L. Aleiner, "Interplay of coulomb and electron-phonon interactions in graphene," Phys. Rev. B 77, 041409 (2008).
- [69] B. Putzer, M. Christos, and M. S. Scheurer, "In preparation," (2023).
- [70] C.-X. Liu, Y. Chen, A. Yazdani, and B. A. Bernevig, "Electron-K-Phonon Interaction In Twisted Bilayer Graphene," arXiv e-prints (2023), 2303.15551 [cond-mat.supr-con].
- [71] E. Khalaf, A. J. Kruchkov, G. Tarnopolsky, and A. Vishwanath, "Magic angle hierarchy in twisted graphene multilayers," Phys. Rev. B 100 (2019), 10.1103/physrevb.100.085109.

Appendix A: Normal-state

1. Hartree-Fock numerics

To capture the non-interacting band structure, we use a continuum-model description [66],

$$\mathcal{H}_{0} = \int d\mathbf{r} \, \psi_{\rho,\ell,\eta,s}^{\dagger}(\mathbf{r}) \left[h_{\eta}(\mathbf{\nabla},\mathbf{r}) \right]_{\rho,\ell;\rho',\ell'} \psi_{\rho',\ell',\eta,s}(\mathbf{r}), \tag{A1}$$

where $\psi_{\rho,\ell,\eta,s}^{\dagger}$ creates an electron of spin $s=\uparrow,\downarrow$, in valley $\eta=\pm$, sublattice $\rho=A,B$, and with pseudo-layer quantum-number $\ell=1,2$; in case of TBG, ℓ refers to the actual two graphene layers, whereas, for TTG, it denotes the two mirror-even layer-eigenstates, $(1,1,1)^T$ and $(1,-2,1)^T$, of the three layers [71]. The continuum model involves two terms, $(h_{\eta})_{\ell,\ell'}=\delta_{\ell,\ell'}h_{\ell,\eta}^{(d)}(\nabla)+(h_{\eta}^{(t)}(r))_{\ell,\ell'}$; the first one, $h_{\ell,\eta}^{(d)}=-i\hbar v_F e^{i\frac{\rho_z\theta_\ell}{2}}(\eta\rho_x\partial_x-\rho_y\partial_y)e^{-i\frac{\rho_z\theta_\ell}{2}}$ with ρ_j being Pauli matrices in sublattice space, describes the Dirac cones of chirality η , rotated by $\theta_\ell=(-1)^\ell\theta/2$ in the two (pseudo)layers ℓ ; the second one, $h^{(t)}$, captures the tunneling between the layers, with amplitude w_0 and w_1 between the same and opposite sublattices, respectively. The modulation of the tunneling on the moiré scale leads to a reconstruction of the band structure, exhibiting nearly flat bands for magic angles around $\theta \simeq 1.1^\circ$ and $\theta \simeq 1.5^\circ$ for TBG and TTG, respectively. We take $w_1=89$ meV, $\frac{w_0}{w_1}=.55$, $v_F=10^6$ m/s, $\theta=1.09^\circ$ in all our numerical calculations.

As already mentioned above, experiments [19, 20] indicate that the superconducting phase in the density regime $2 < |\nu| < 3$ coexists with the reset behavior at half-filling, $|\nu| = 2$, of the upper or low flat-bands. To model this effect, we add Coulomb repulsion,

$$\mathcal{H}_C = \frac{1}{2N} \sum_{\mathbf{q}} V(\mathbf{q}) \rho_{\mathbf{q}} \rho_{-\mathbf{q}}$$
 (A2)

to our Hamiltonian, where ρ_q is the Fourier transform of the density of the continuum-model electrons c_r and the N the number of moiré unit cells. We assume a double gate screened Coulomb potential of the form:

$$V(\mathbf{q}) = \frac{1}{A_m} \frac{1 - e^{-2d_s|\mathbf{q}|}}{2\epsilon\epsilon_0|\mathbf{q}|} \tag{A3}$$

In the above, A_m is the area of a real-space moiré unit cell (since we consider TBG and not TTG in our numerics, we take A_m to be the moiré unit cell for 1.09°), d_s is the screening distance which we take to be 40 nm, and ϵ is the dielectric constant we take to be $\epsilon \simeq 4$. Note that projecting Eq. (A2) into the bands of TTG will also lead to interactions coupling the mirror-sectors. However, as was shown [13] analytically in a specific limit and numerically for realistic parameters, also the interacting physics of TTG decays into that of the TBG and that of a single Dirac cone for $D_0 = 0$. As such, it is justified to focus on the mirror-bands as in Eq. (A1) when discussing the reset physics in TTG at $D_0 = 0$.

In computing the normal state, we assume the same normal state density matrix as in Ref. 13 where the expectation value $\langle c^{\dagger}_{\mathbf{k},\alpha,\eta}c^{\dagger}_{-\mathbf{k},\beta,\eta}\rangle$ is equal to the $\frac{1}{2}$ Id in the subspace of the flat bands of one spin flavor which are half filled in our normal state and equal to Id in the flat bands of the remaining spin flavor which are fully polarized. We emphasize that we are assuming a static, momentum independent ansatz for the normal state density matrix which is not obtained self consistently. As can be seen in Fig. 2, instead of just rigidly shifting one spin species away from the Fermi level, there are also significant band renormalizations, in particular for the active spin flavor. Similar to the toy model with t' < 0 used in Fig. 1, the Dirac cones at the K and K' points are pushed towards the top of the bands.

2. Gauge Fixing

We will also describe how we fix the phases of the continuum model Bloch wavefunctions we use in our computations. We denote the wavefunction of band n in valley η at momentum k by $u_{k,n,\eta}$. We use $C_{2z}\mathcal{T}$ to fix the phase of the wavefunctions to be either +1 or -1 by enforcing:

$$C_{2z}\mathcal{T}u_{\mathbf{k},n,\eta} = u_{\mathbf{k},n,\eta} \tag{A4}$$

We then fix the relative sign of wavefunctions in opposite flat bands but the same valley with the chiral symmetry operator C as:

$$Cu_{\mathbf{k},\pm,\eta} = i\eta \pm u_{\mathbf{k},\mp,\eta} / |\langle u_{\mathbf{k},\pm,\eta}^* | C | u_{\mathbf{k},\pm,\eta} \rangle|$$
(A5)

We fix the relative sign of wavefunctions in opposite bands and opposite valleys with PHC_{2z} , where PH a unitary particle hole symmetry operator with:

$$PHC_{2z}u_{\mathbf{k},\pm,\eta} = i\eta u_{\mathbf{k},\mp,-\eta} \tag{A6}$$

Finally, we use time-reversal symmetry to fix the relative sign between wavefunctions at opposite k, in opposite valleys, but within the same band:

$$\mathcal{T}u_{\mathbf{k},n,\eta} = u_{-\mathbf{k},n,-\eta} \tag{A7}$$

Appendix B: Gap Equation at T=0

In this appendix we will discuss the self consistency equations we solve to obtain our T=0 solutions. In general, we write the Hamiltonian in a Nambu basis as:

$$\mathcal{H}_{\mathbf{k}} = \begin{pmatrix} c_{\mathbf{k},+}^{\dagger} & c_{-\mathbf{k},-} \end{pmatrix} \begin{pmatrix} \xi_{\mathbf{k},+} & \Delta(\mathbf{k}) \\ \Delta(\mathbf{k})^{\dagger} & -\xi_{-\mathbf{k},-} \end{pmatrix} \begin{pmatrix} c_{\mathbf{k},+} \\ c_{-\mathbf{k},-}^{\dagger} \end{pmatrix}$$
(B1)

Where we have suppressed spin and band indices, and both $\xi_{k,\pm}$ and Δ_k are matrices in band and spin space. $\xi_{k,\pm}$ represents the normal state dispersion in the \pm valleys, which we take to be spin polarized and renormalized by Coulomb interactions as described in App. A. Δ_k can be expressed as:

$$\Delta_{\mathbf{k}}^{\alpha,\eta;\beta,-\eta} = \frac{1}{N} \sum_{\mathbf{k},\mathbf{k'}} \chi_{\mathbf{k},\mathbf{k'}} \lambda_{\mathbf{k},\mathbf{k'}}^{\alpha,\eta;\gamma,\eta'} \left(\langle c_{-\mathbf{k}} c_{\mathbf{k}} \rangle^T \right)^{\gamma,\eta';\delta,-\eta'} \left(\lambda_{-\mathbf{k},\mathbf{k'}}^T \right)^{\delta,-\eta';\beta,-\eta}$$
(B2)

In the above, $\lambda_{k,k'}^{\alpha,\eta;\gamma,\eta'}$ represent form factors of some matrix elements which could represent either phonons or fluctuations projected into the flat bands and may be valley diagonal or off diagonal. $V_{k,k'}$ is an isotropic potential which we will generally take to be attractive and flat for phonons and attractive with some lorentzian form for fluctuation mediated pairing. Since we will be assuming interactions with strength less than the scale of the coulomb interactions, we will treat the polarized spin flavor which is fully occupied at $\nu = 2$ as a spectator and assume the pairing is zero in these bands. The self consistency condition we solve at T = 0 is:

$$\langle c_{-\mathbf{k},\alpha,-}c_{\mathbf{k},\beta,+}\rangle = U_{\mathbf{k}}^* \chi_{\mathbf{k}} U_{\mathbf{k}}^T \tag{B3}$$

Where $U_{\mathbf{k}}$ is defined as the unitary operator such that:

$$U_{\mathbf{k}}^{\dagger} \mathcal{H}_{\mathbf{k}} U_{\mathbf{k}} = D_{\mathbf{k}} \tag{B4}$$

Here, D_{k} is a diagonal matrix with the Fermi-Dirac functions of eigenvalues of \mathcal{H}_{k} at T=0 as its diagonal entries. χ_{k} is the matrix with Fermi-Dirac functions at T=0 K of the entries of D on the diagonal. We also must impose Fermi-Dirac statistics as a constraint on our solutions. We enforce this constraint at each iteration by splitting $\langle c_{-k,\alpha,-}c_{k,\beta,+}\rangle$ into components which go as either η_{x} in valley space (denoted E_{k}) or η_{y} in valley space (denoted as O_{k}) depending on whether the pairing is even or odd under $k \to -k$ and the antisymmetry or symmetry of the band indices as:

$$O_{\mathbf{k}} = \frac{1}{2} \left(\langle c_{-\mathbf{k},\alpha,-} c_{\mathbf{k},\beta,+} \rangle + \langle c_{\mathbf{k},\beta,-} c_{-\mathbf{k},\alpha,+} \rangle \right) \qquad E_{\mathbf{k}} = \frac{1}{2} \left(\langle c_{-\mathbf{k},\alpha,-} c_{\mathbf{k},\beta,+} \rangle - \langle c_{\mathbf{k},\beta,-} c_{-\mathbf{k},\alpha,+} \rangle \right)$$
(B5)

Our iterative procedure then proceeds as follows. At the zeroth iteration, an ansatz for $\langle c_{-\mathbf{k},\alpha,-}c_{\mathbf{k},\beta,+}\rangle$ satisfying the desired symmetries is selected. Then at each iteration, the chemical potential is adjusted to give the desired filling, which we take to be $\nu=2.5$ in our numerics. $U_{\mathbf{k}}$ and the resulting functions $O_{\mathbf{k}}$ and $E_{\mathbf{k}}$ are then computed and plugged back into $\Delta_{\mathbf{k}}$, (which also is guaranteed to obey Fermi-Dirac statistics assuming our generalized form factors obey time reversal symmetry). $\Delta_{\mathbf{k}}$ is then used to compute the new $U_{\mathbf{k}}$, and the procedure is repeated until convergence is reached in $\Delta_{\mathbf{k}}$ and μ . In practice, in our T=0 numerics, we take $\mathbf{q}=\mathbf{k}-\mathbf{k'}$ to only be summed over the first Brillouin zone, an assumption justified for our fluctuation mediated SC by $\chi(\mathbf{q})$ falling off as $\frac{1}{|\mathbf{q}|^2}$ near the first Brillouin zone edge.

Appendix C: Gap Equation at T_c

In this appendix, we will describe how we compute solutions to the linearized gap equation at T_c . As in App. B, we will assume a spin polarized normal state and only consider superconducting instabilities within a single spin flavor. We recall that for the case of fluctuation-mediated superconductivity, we couple electrons to bosonic modes (j = 1, 2, ...) as, e.g., in Eq. (4), with $\lambda^j_{\alpha,\eta;\alpha',\eta'}$ capturing the symmetries broken by the corresponding order parameter. In order to compactly write down the linearized gap equation, it is convenient to express λ^j as

$$\left(\lambda_{\alpha,\eta;\alpha',\eta'}^{j}\right)_{\mathbf{k},\mathbf{k}'} = A_{\mathbf{k},\mathbf{k}'}^{\alpha,\eta;\alpha',-\eta}\delta_{\eta,-\eta'} + B_{\mathbf{k},\mathbf{k}'}^{\alpha,\eta;\alpha',\eta}\delta_{\eta,\eta'}. \tag{C1}$$

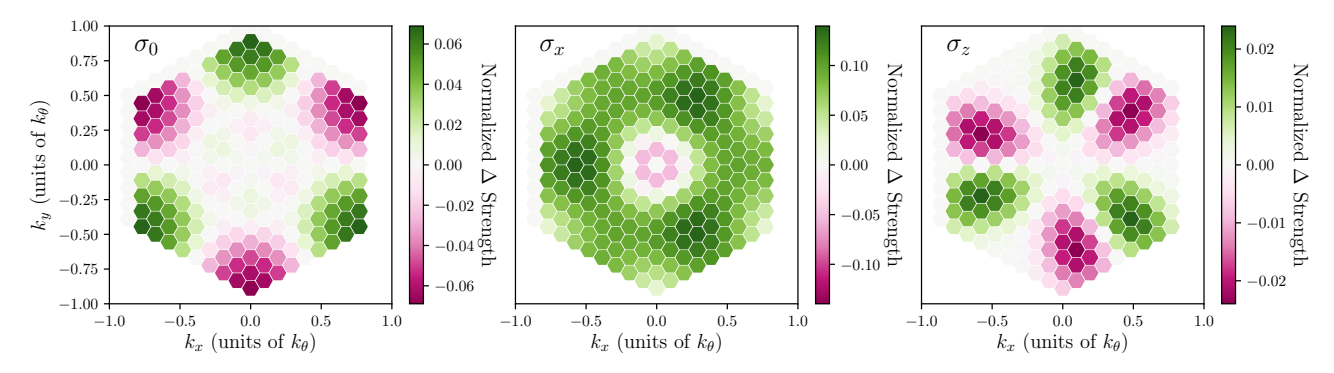


FIG. 5: Highest eigenvalue pairing obtained from linearized gap equation at T=16 K, for SLP- and T-IVC fluctuations. The pairing transforms under the B_2 representation of the point group.

Here we also include the momentum dependence of the matrix elements, which arises when we study phonons and order parameter fluctuations projected from the sublattice basis to the band basis. In Eq. (C1), $A_{k,k'}$ are the valley off diagonal pieces of the form factor $\lambda^j_{\alpha,\eta;\alpha',\eta'}$ and $B_{k,k'}$ is the valley diagonal pieces. With this notation in hand, the linearized gap equation we solve is

$$\left(\Delta(\mathbf{k})^{\dagger}\right)^{\alpha,-;\beta+} = -\sum_{\mathbf{q}} V_{\mathbf{q}} \left(\mathcal{G}_{\mathbf{k}-\mathbf{q}}^{\delta-;\gamma+} B_{\mathbf{k}-\mathbf{q},\mathbf{q}}^{\gamma+;\beta+} (B_{-\mathbf{k}+\mathbf{q},-\mathbf{q}}^{T})^{\alpha-;\delta-} - \mathcal{G}_{-\mathbf{k}+\mathbf{q}}^{\gamma-;\beta+} A_{\mathbf{k}-\mathbf{q},\mathbf{q}}^{\gamma-;\beta+} (A_{-\mathbf{k}+\mathbf{q},-\mathbf{q}}^{T})^{\alpha-;\delta+} \right), \tag{C2}$$

where the Greens function $\mathcal{G}_{k-q}^{\alpha+;\beta-}$ defined by

$$\mathcal{G}_{\mathbf{k}}^{\alpha+;\beta-} = \frac{1}{A} \left(\frac{\Delta_{\mathbf{k}}^{00}}{2|\xi_{\mathbf{k},0}|} \left(1 - 2n_F(|\xi_{\mathbf{k},-}|) \right) (\sigma_0 + \sigma_z)^{\alpha\beta} + \frac{\Delta_{\mathbf{k}}^{11}}{2|\xi_{\mathbf{k},1}|} \left(1 - 2n_F(|\xi_{\mathbf{k},+}|) \right) (\sigma_0 - \sigma_z)^{\alpha\beta} + \frac{\Delta_{\mathbf{k}}^{01} + \Delta_{\mathbf{k}}^{10}}{\xi_{\mathbf{k},0} + \xi_{\mathbf{k},1}} (n_F(-\xi_{\mathbf{k},1}) - n_F(\xi_{\mathbf{k},0})) (\sigma_x + i\sigma_y)^{\alpha\beta} + \frac{\Delta_{\mathbf{k}}^{01} - \Delta_{\mathbf{k}}^{10}}{\xi_{\mathbf{k},0} + \xi_{\mathbf{k},1}} (n_F(-\xi_{\mathbf{k},1}) - n_F(\xi_{\mathbf{k},0})) (\sigma_x - i\sigma_y)^{\alpha\beta} \right).$$
(C3)

Here $\Delta_{\mathbf{k}}^{\alpha\beta}$ denote the pairing in band space where $\alpha, \beta = 0, 1$ label the upper and lower flat band.

Finding a solution to the above equation then amounts to computing the right-hand side of Eq. C2, diagonalizing it in the space of momenta, Nambu index, and band index, and looking at the eigenvectors which attain eigenvalue 1 for some value of T. To enforce Fermi-Dirac statistics, we solve the above equation on half of the moiré Brillouin zone.

Appendix D: More Superconducting Instabilities

In this appendix, we will discuss the superconducting instabilities we find beyond the A_2 and B_1 states shown in Figs. 2 and 3 and focus on the other leading instabilities we find in the presence of fluctuations of different particle hole orders. For SLP- fluctuations, we find the B_2 state can be favored over the B_1 when the strength of T-IVC fluctuations are on the same order as SLP- fluctuations, as shown in Fig. 4. We show the B_2 state for parameter value $\theta_{fluc.} \simeq \frac{\pi}{4}$ in Fig. 5. For N-IVC fluctuations as well as for SLP- fluctuations, we find the E_2 is the leading instability, as shown in Fig. 4. We show the two components of the E_2 state for parameter value $\theta_{fluc.} \simeq \frac{\pi}{2}$ in Fig. 5. We point out that each component of the E_1 pairing shown in Figs. 6 and 7 may by themselves be nodal, assuming the pieces of each pairing which are proportional to σ_x in band space are smaller than the band splitting. In general, we expect the lowest energy pairing at T=0 will be the chiral E_1 state which would be fully gapped; however, in the presence of sufficient strain, a single basis function of the E_1 pairing can be favored over the chiral state; offering another route to nodal superconductivity in the presence of N-IVC fluctuations.

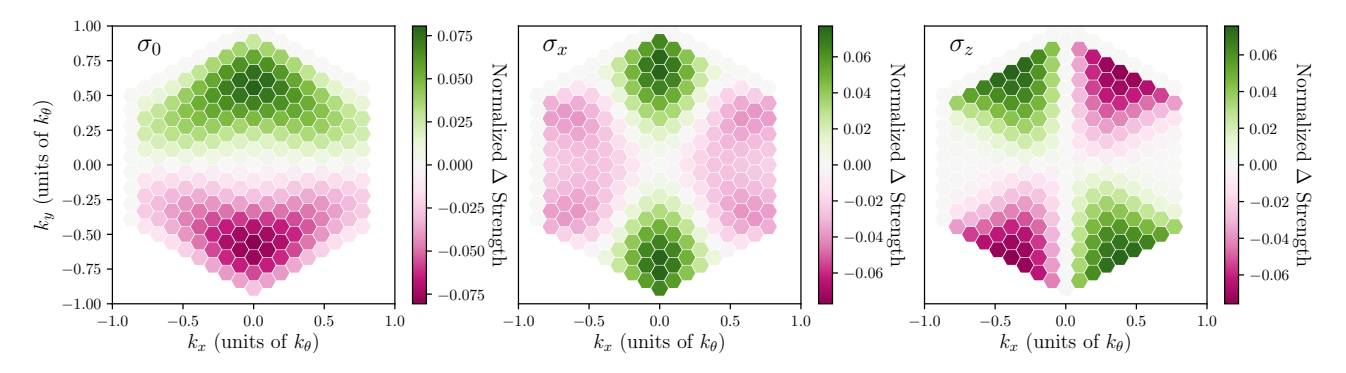


FIG. 6: First component of the highest eigenvalue pairing obtained from linearized gap equation at T = 16 K for just N-IVC fluctuations. The pairing transforms under the E_1 representation of the point group. The component shown here is degenerate with the other basis functions which transform under C_3 symmetry shown in Fig. 7.

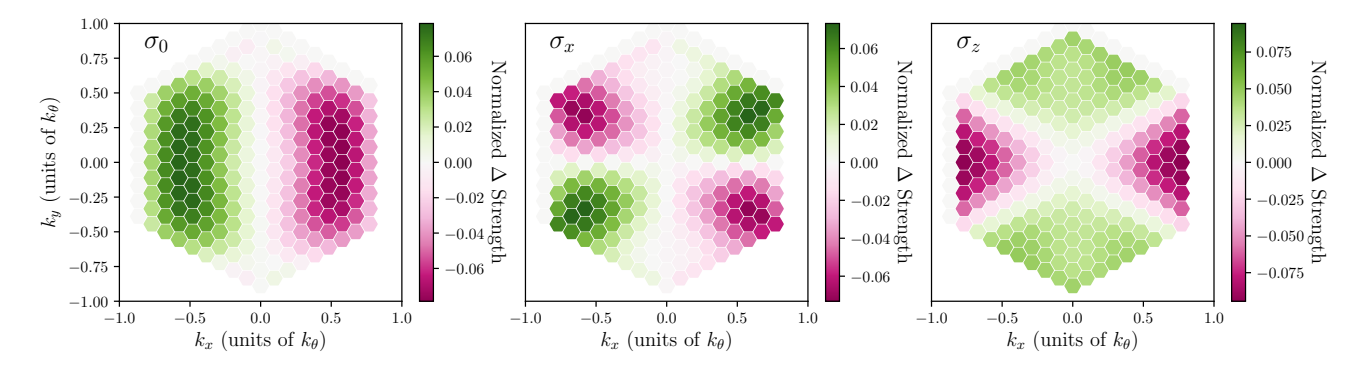


FIG. 7: Second component of the highest eigenvalue pairing obtained from linearized gap equation at T = 16 K for just N-IVC fluctuations. The pairing transforms under the E_1 representation of the point group. The component shown here is degenerate with the other basis functions which transform under C_3 symmetry shown in Fig. 6.